PERGAMON

PII: S1359-6454(98)00409-1

ON THE FATIGUE BEHAVIOR OF γ-BASED TITANIUM ALUMINIDES: ROLE OF SMALL CRACKS

J. J. KRUZIC, J. P. CAMPBELL and R. O. RITCHIE†

Materials Sciences Division, Lawrence Berkeley National Laboratory, and Department of Materials
Science and Mineral Engineering, University of California, Berkeley, CA 94720-1760, U.S.A.

Abstract—Gamma-TiAl based alloys have recently received attention for potential elevated temperature applications in gas-turbine engines. However, although expected critical crack sizes for some targeted applications (e.g. gas-turbine engine blades) may be less than $\sim 500\,\mu$m, most fatigue-crack growth studies to date have focused on the behavior of large (on the order of a few millimeters) through-thickness cracks. Since successful implementation of damage-tolerant life-prediction methodologies requires that the fatigue properties be understood for crack sizes representative of those seen in service conditions, the present work is focused on characterizing the initiation and growth behavior of small ($a \sim 25$–$300\,\mu$m) fatigue cracks in a γ-TiAl based alloy, of composition Ti–47Al–2Nb–2Cr–0.2B (at.%), with both duplex (average grain size of $\sim 17\,\mu$m) and refined lamellar (average colony size of $\sim 145\,\mu$m) microstructures. Results are compared to the behavior of large ($a > 5$ mm), through-thickness cracks from a previous study. Superior crack initiation resistance is observed in the duplex microstructure, with no cracks nucleating after up to 500 000 cycles at maximum stress levels ($R = 0.1$) in excess of the monotonic yield stress, σ_y. Comparatively, in the lamellar microstructure cracks nucleated readily at applied maximum stresses below the yield stress (85% σ_y) after as few as 500 cycles. In terms of crack growth, measurements for small fatigue cracks in the duplex and lamellar microstructures showed that both microstructures have comparable *intrinsic* fatigue-crack growth resistance in the presence of small flaws. This observation contrasts previous comparisons of large-crack data, where the lamellar structure showed far superior fatigue-crack growth resistance than the duplex structure. Such "small-crack effects" are examined both in terms of similitude (i.e. crack tip shielding) and continuum (i.e. biased microstructural sampling) limitations of traditional linear elastic fracture mechanics. © *Published by Elsevier Science Ltd on behalf of Acta Metallurgica Inc.*

1. INTRODUCTION

Gamma-TiAl based intermetallic alloys have received considerable attention of late as candidate materials for high-temperature aerospace and automotive applications [1, 2]. In comparison to conventional gas-turbine engine materials [1–4], titanium aluminides composed primarily of the γ-phase possess ~ 15 and 50% lower density than conventional titanium and nickel alloys, respectively, while maintaining adequate oxidation resistance, creep resistance and elevated-temperature strength retention. Indeed, specific compositions and microstructures are reported to be capable of satisfactory performance at operating temperatures up to $\sim 760^\circ$C [2, 4], and thus offer the potential of improved engine efficiency and performance via higher operating temperatures and improved thrust-to-weight ratios.

Of particular interest have been two-phase materials with the alloy composition (in at.%) Ti–47Al–2Nb–2Cr, which have γ-TiAl (ordered $L1_o$

structure) as the majority phase and α_2-Ti$_3$Al phase (ordered $D0_{19}$ structure) as the secondary phase. These alloys are invariably processed to either a *duplex* microstructure, consisting of equiaxed grains of γ with small amounts of α_2 grains, or a *lamellar* microstructure consisting of lamellar colonies containing alternating γ and α_2 platelets. The lamellar microstructures can be up to two orders of magnitude coarser, with colony sizes ranging from 100 to 2000 μm, compared to grain sizes of 10–50 μm in duplex microstructures.

With respect to mechanical properties, these alloys have ambient-temperature tensile strengths on the order of 500–600 MPa,‡ yet limited damage tolerance in the form of low ductility (e.g. less than a few percent) and low *crack-initiation* fracture toughness (~ 10–18 MPa $\sqrt{\text{m}}$). In general, duplex microstructures display better elongation (up to ~ 4 vs 1% in lamellar structures) and slightly higher strengths, whereas lamellar microstructures show better creep resistance and have higher toughness, specifically in the form of more pronounced (large-crack) *R*-curve behavior [1, 2, 6–9].

The issue of fatigue resistance, however, is more complex. Although the duplex structures appear to have somewhat higher fatigue limits [4, 10] based on

---

†To whom all correspondence should be addressed.
‡Much higher tensile strengths (exceeding 1000 MPa) have been developed in P/M alloys with lamellar microstructures, where the γ lath widths have been refined from ~ 1–2 to $\sim 0.1\,\mu$m [5].

smooth-bar stress/life (S/N) testing, conventional fatigue-crack growth properties [measured using standard, *large-crack* specimens containing through-thickness (>5 mm) cracks] are clearly superior in the lamellar structures [4, 9, 11–14], e.g. large-crack fatigue threshold values, ΔK_{TH}, are up to ~50% higher than in the duplex structures. However, as will be shown, this benefit is lost when tests are performed on small ($\lesssim 500 \, \mu$m) surface cracks. In fact, the small-crack growth properties of the two microstructures are quite similar. Indeed, the duplex structure may actually be considered to exhibit preferable small-crack fatigue properties, as there is an easily definable small-crack threshold (such a threshold is not readily defined for lamellar structures) and there is far less scatter in the crack-growth data (due to the finer scale of the duplex microstructure).

For many potential applications of titanium aluminides, such as gas-turbine engine components, fatigue design will most likely be based on a fatigue-threshold condition, as crack-propagation lives will inevitably be very short. This follows from the strong dependence of crack-growth rates on the stress-intensity range (i.e. high exponents, $m \sim 9$–22, in the Paris law [13]), typical of intermetallics [9, 11, 15, 16], which results in short (crack-propagation) lives in terms of the *number of cycles* to failure. Furthermore, in the case of engine blade applications, the vibratory loading frequencies are extremely high (>1 kHz) [17, 18], leading to a short fatigue life in terms of the *time* to failure.

Accordingly, the aim of this work is to characterize the initiation and growth of small (half-surface crack length, $c \sim 25$–300 μm) cracks in duplex and lamellar microstructures in a γ-TiAl based alloy, and by comparison to existing results for large (>5 mm) cracks [12, 13], explain the differing role of microstructure in affecting large- and small-crack behavior.

2. BACKGROUND

For successful implementation of damage-tolerant design and life-prediction methodologies, it is important that the fatigue properties are defined for crack sizes comparable to those seen in service. This is important since cracks that are physically small (typically $\lesssim 500 \, \mu$m in size) can behave quite differently than larger cracks, in that their growth rates can be far in excess of corresponding large cracks subjected to the same applied driving force, and they can propagate at applied stress intensities *less than* the fatigue threshold, ΔK_{TH}, below which large cracks are presumed to be dormant. Small-crack

effects are typically seen when crack sizes become comparable to [19, 20]:

1. the characteristic dimensions of the microstructure (a continuum limitation);
2. the extent of local inelasticity (e.g. the plastic-zone size) *ahead* of the crack tip (a linear-elastic fracture mechanics limitation);
3. the extent of the zone of crack-tip shielding *behind* the crack tip (a similitude limitation).

With respect to γ-TiAl based intermetallics, the continuum and similitude limitations are of most importance, particularly in the case of the coarse lamellar structures. In such microstructures, colony sizes can be as large as several millimeters, such that crack sizes can readily approach microstructural dimensions. Moreover, crack-growth resistance in the lamellar structures can be enhanced by uncracked (shear) ligament bridging (both for monotonic [7] and cyclic [12] loading); since this is a shielding mechanism that operates principally behind the crack tip, it becomes far less effective for crack sizes smaller than the equilibrium bridging-zone length. Despite the importance of small-crack effects in γ-TiAl based intermetallic alloys, both from the point of view of mechanisms and applications, only a limited amount of small-crack fatigue data has been collected on lamellar microstructures [14, 21–24] with very little attention given to duplex microstructures [21]. Furthermore, little or no information is available on the nucleation of small fatigue cracks or the origins of the small-crack effects in these alloys.

3. EXPERIMENTAL PROCEDURES

3.1. Material, microstructures and mechanical properties

Duplex and lamellar microstructures were studied in a γ-titanium aluminide based alloy, of composition Ti–47Al–2Nb–2Cr–0.2B (at.%);† the B additions resulted in ~0.5 vol.% of needle-like TiB$_2$ particles (~2–10 μm in length and ~1 μm in diameter). The lamellar microstructure [Fig. 1(a)] was obtained by forging and subsequent heat treating at 1370°C in flowing argon for 1 h, air cooling and then holding 6 h at 900°C prior to argon furnace cooling. The resulting microstructure consisted of ~145 μm-sized lamellar colonies with very small amounts (~4%) of fine equiaxed γ grains (5–20 μm) between lamellar colonies; the α_2 spacing (center-to-center) in the lamellar region was ~1.3 μm. The corresponding duplex microstructure [Fig. 1(b)] was achieved by forging and subsequent heat treating at 1320°C in argon for 3 h, followed by argon furnace cooling. This microstructure consisted of nearly equiaxed grains of the γ-phase, ~17 μm in diameter, with the α_2 phase appearing along γ grain boundaries and at triple points. Both the lamellar and
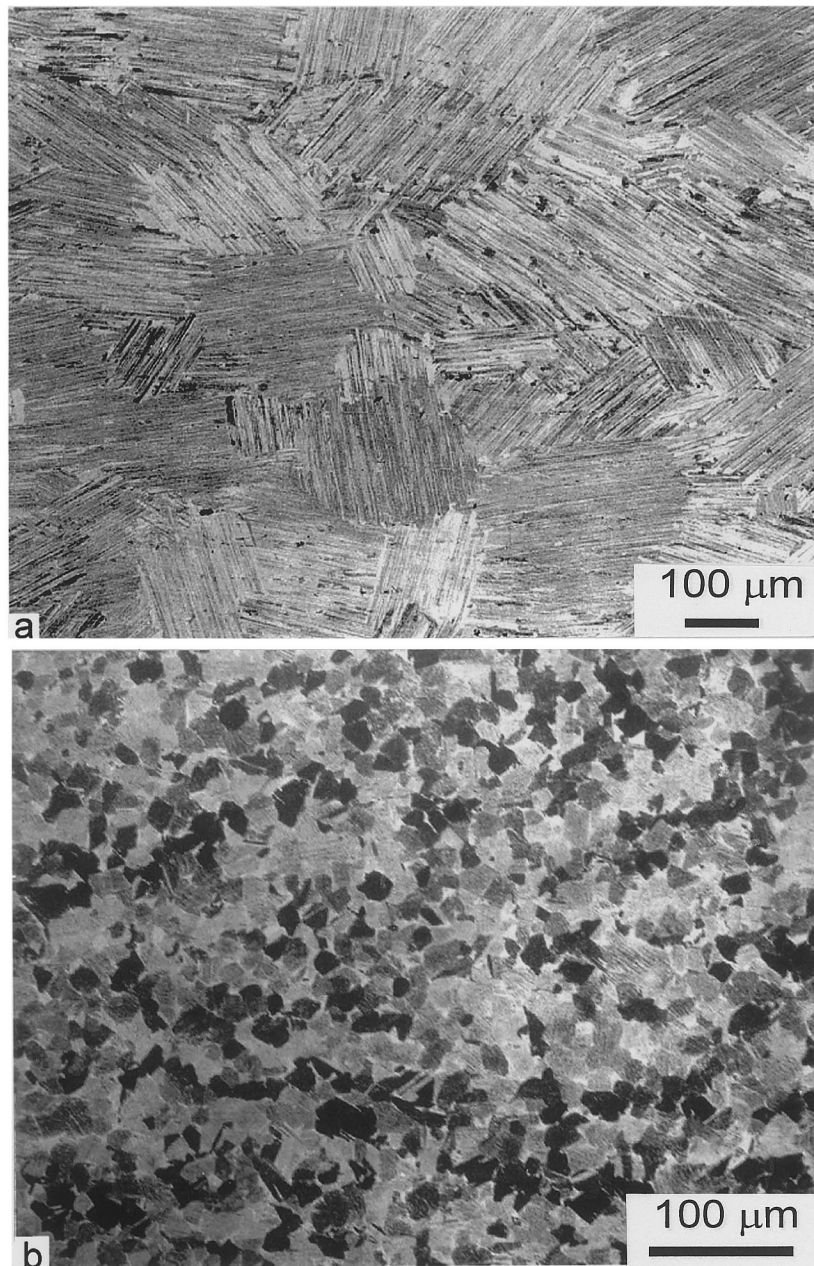
Fig. 1. Optical micrographs of the lamellar (a) and duplex (b) microstructures of a Ti–47Al–2Nb–2Cr–0.2B (at.%) alloy. (Etched with 2% HF, 5% H_3PO_4 etchant.)

duplex microstructures contained approximately 10 vol.% of the α_2 phase.

The ambient-temperature mechanical properties of these two microstructures are listed in Table 1.

3.2. Small-crack fatigue testing

3.2.1. Crack initiation. The initiation of small surface cracks was evaluated in room temperature air using unnotched, 6 mm thick, rectangular beams loaded in four-point bending. The process of natural fatigue-crack initiation was observed by periodically interrupting the test, at which time cracks were either observed directly on the sample surface or on surface replicas. Replication was performed with the sample under load using cellulose acetate tape softened with acetone. The replicas were then gold or platinum coated to improve resolution and the corresponding crack lengths were measured using optical microscopy. With such techniques, the nucleation of cracks as small as a few microns could be detected, while the early growth of crack sizes as small as 25 μm could be monitored.

Small surface cracks were also initiated from electro-discharge machining (EDM) pit damage generated on the tensile-loaded beam surface; the rapid, localized heating and cooling associated with the

Table 1. Mechanical properties of duplex and lamellar microstructures

Microstructure	Yield stress, σ_y (MPa)	Fracture strength (MPa)	Elongation (%)	Fracture toughness† (MPa $\sqrt{m}$)
fully lamellar	426	541	0.8	18–30
duplex	384	489	0.94	‡

†The range in values indicates *R*-curve behavior; the first value corresponds to the crack-initiation toughness, K_i, the second to the steady-state toughness or maximum measured crack-growth resistance, K_{ss}. ‡Although fracture toughness was not measured for the present duplex material, studies on similar materials indicate single values of $K_i \sim 10$ MPa $\sqrt{m}$ with no *R*-curve behavior [9, 25].

electrical discharge produced small cracks a few hundred microns long in the vicinity of the pit and extending from the pit. Samples were then cyclically loaded to grow the cracks away from the heat-affected zone (HAZ) prior to data acquisition (Fig. 2); the HAZ was easily identified optically using an aqueous 2% HF, 5% H_3PO_4 etchant on a polished surface. In some instances, sample surfaces were ground and polished following pitting to partially or completely eliminate the EDM damage, leaving only small surface cracks that originated from the pitting process. Using such procedures, initial half-surface crack lengths less than $c \sim 120\ \mu m$ were readily achieved.

In an attempt to obtain smaller, artificially induced, initial flaw sizes, laser ablation was also used to create damage sites on samples of both microstructures. A three-nanosecond laser was used with a wavelength of 266 nm to create pits on the surface of the samples. The laser beam was focused and pulsed 2–3 times to give initial pit sizes of 20–40 μm in diameter. During the pitting process, ma-

terial was vaporized, forming a pit, with the vaporized material being redeposited on the surface surrounding the newly formed pit. This redeposited material was polished off to leave a smooth surface around a well-defined pit with the HAZ limited to a few microns, as observed by optical microscopy. In general these laser-induced pits were too small to initiate cracking, with only one exception, where a crack in the duplex microstructure did grow from a laser ablation pit. In the lamellar microstructure, the sampling volume of the 20–40 μm diameter stress concentrators was insufficient to produce crack initiation in the vicinity of the pit; cracks initiated naturally elsewhere.

3.2.2. Fatigue-crack growth measurements. Fatigue-crack growth measurements were conducted on small surface fatigue cracks ranging in surface half-lengths from $c \sim 25$–300 μm. Samples were cycled at a positive load ratio, $R = K_{min}/K_{max}$, of 0.1 at frequencies between 5 and 25 Hz (sine wave). Similar to crack initiation, crack lengths were measured by optical microscopy of Au- or Pt-coated replicas,
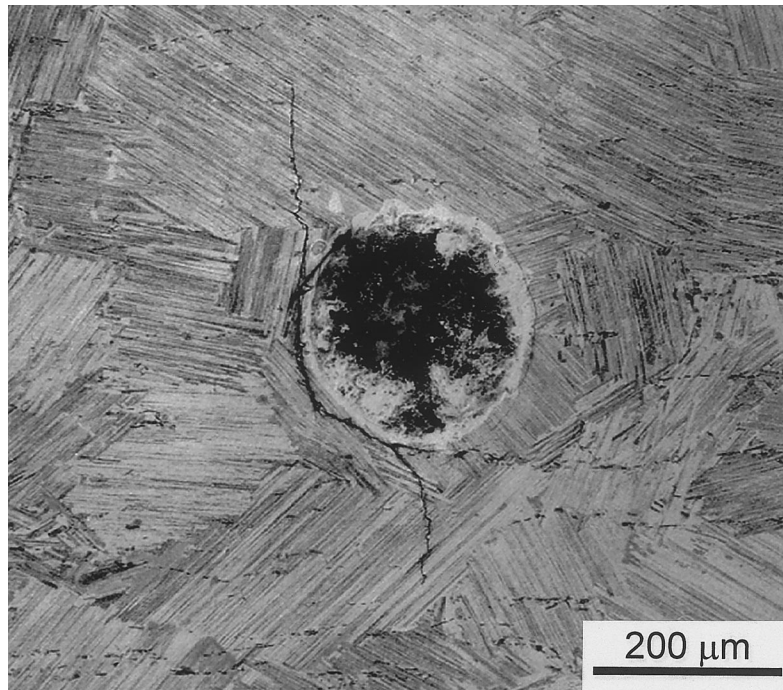

Fig. 2. Optical micrograph of an EDM pit and resulting microcrack, which has grown from the pit due to cyclic loading. (Etched with 2% HF, 5% H_3PO_4 etchant.)

periodically taken at the tensile surface of the sample. Growth rates were then computed from the amount of crack extension between two discrete measurements (replicas). Stress intensities were determined using linear-elastic solutions for surface cracks in bending [26]. A semi-circular crack profile was assumed, i.e. a crack depth to half-surface crack length ratio of $a/c = 1$ (Fig. 3). This assumption was verified by heat tinting specific samples at $600°C$ to create a layer of bright blue oxide product on the crack surface; after fracturing the samples, an average a/c ratio of 1.03 was observed. In this regard, it has been noted that surface cracks grown in bending show a tendency to decrease in a/c ratio significantly with increasing a/t [27, 28], where t is the "width" of the beam (Fig. 3); however, in the present study, this effect was insignificant as a/t ratios were small throughout the duration of each test ($a/t < 0.02$).

4. FATIGUE-CRACK INITIATION

4.1. Lamellar microstructure

4.1.1. Crack nucleation. Small cracks were found to initiate readily in the lamellar microstructure when maximum bending stresses ($R = 0.1$) were below the tensile yield stress (85% of σ_y), with cracks initiating primarily in lamellar colonies that were favorably oriented with respect to the maximum tensile stress direction (i.e. the long axis of the beam). Defining the angle between the lamellar interfaces and the maximum tensile stress direction as β, the following observations can be made regarding crack nucleation at specific stress ranges between 300 and 500 MPa.

- Cracks most commonly formed in colonies where β was $\sim 90°$ or $45°$; these angles correspond to the orientations of maximum tensile and shear stresses, respectively, on the lamellar interfaces.
- For colonies with $\beta \sim 90°$, many cracks were observed to initiate within the first 500 cycles.
- For $\beta \sim 45°$, shear deformation bands were observed to form within the first 500 cycles. The number of cycles necessary to subsequently initiate cracks along shear bands varied greatly (from 500 to $> 10\,000$ cycles at a specific stress range).
- Cracks were also observed to initiate in colonies with β between $45°$ and $90°$; however, the majority of cracks were observed to form within $\sim 15°$ of the maximum tensile or shear orientations.
- Initial crack nucleation was not observed in colonies where β was significantly less then $45°$.

As applied stress ranges were increased, new cracks and shear bands were observed to nucleate, again with crack initiation occurring within the first 500 cycles (at the increased load) within favorably oriented colonies (i.e. interfaces perpendicular to the maximum tensile stress direction, $\beta \sim 90°$) and along both newly created and previously existing shear bands with varied amounts of cycling.

Fatigue-crack initiation tended to occur parallel to the lamellar interfaces, with the nucleated cracks extending partially or completely across the lamellar colonies; most commonly many cracks of various sizes formed within individual favorably oriented colonies (Fig. 4). Such cracks did not necessarily lie entirely on a single interface or lamellae; rather, cracks would often jump to adjacent interfaces or lamella. Since cracking occurred both at the interfaces and jumping between the interfaces along the length of the crack, no determinations were made on the exact locations (intra- or interlamellar or at γ/α_2 boundaries or γ/γ twin interfaces) of the nucleation events. Figure 4 shows a main fatigue crack that runs parallel to the lamellar interfaces for the entire width of the colony, with the crack arrested at both ends. This crack remained arrested as shown for $\sim 70\,000$ cycles after initiation until the sample ultimately failed at another location. Additionally, many small cracks also can be seen that nucleated parallel to the main crack within the same colony. Details regarding the formation of secondary cracks ahead of the main crack tip, as observed in Fig. 4, are discussed below.

4.1.2. Secondary crack formation. Secondary cracks were frequently observed in neighboring colonies ahead of arrested main crack tips, as well as adjacent to or ahead of growing dominant cracks. Secondary cracks either linked up with main
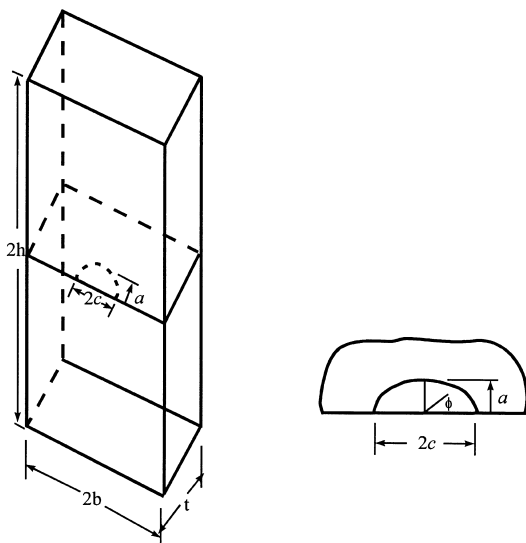
Fig. 3. Schematic showing the small-crack configuration used for the Newman–Raju stress-intensity solution [26] for a semi-elliptical surface crack.
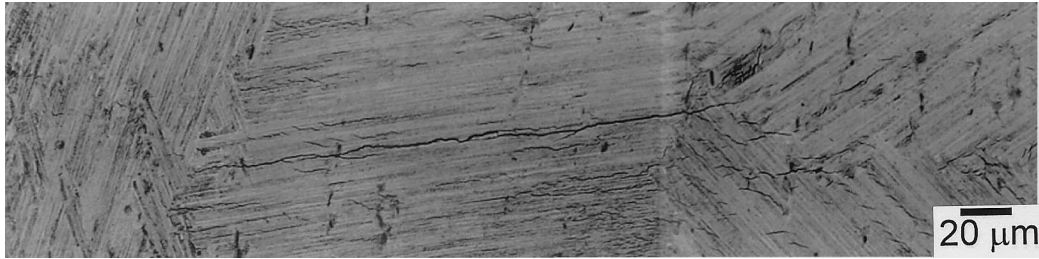
Fig. 4. A backscattered SEM micrograph showing a crack that has nucleated in the lamellar micro-structure and arrested at colony boundaries. Microcracking is apparent ahead of the right crack tip, while no microcracking is seen ahead of the left crack tip. The maximum tensile stress direction was vertical with respect to the orientation of the micrograph.

cracks upon growth or were simply left in the wake of growing, dominant cracks as seen in Fig. 5. In Fig. 4, microcracking is observed in the colonies to the right of the arrested main crack tip, where $\beta \sim 40°$–$50°$. The formation of such secondary cracks to the right of the main crack is consistent with previously documented observations of the mechanism for uncracked ligament bridge formation during fatigue propagation of large cracks in lamellar alloys [9, 13, 29]. To the left of the main crack tip in Fig. 4, no secondary cracking is observed in neighboring colonies; note that the lamellar interfaces in the adjacent colonies are oriented at a low angle to the maximum tensile stress direction ($\beta \sim 0$).

The above observations of secondary crack formation (or lack thereof) to the right and left of the main crack shown in Fig. 4 are consistent with previous reports regarding the influence of lamellae orientation on fatigue-crack growth resistance. Specifically, it has been demonstrated that crack-growth resistance is highest when the crack propagates perpendicular to the lamellar interfaces, while resistance is lowest when the crack is at a low angle to the interface [30–32]. Accordingly, it would seem that the left-hand crack tip is unable to traverse the colony boundary due to the high angle of the lamel-

lar interfaces relative to the crack. Furthermore, the low angle of the lamellar interfaces relative to the maximum tensile stress direction has inhibited secondary crack formation.

Although, as mentioned previously, initial crack nucleation was not observed for β significantly less than $45°$, secondary cracks did sometimes form in colonies unfavorably orientated for crack nucleation ($\beta < 45°$), provided that these colonies were ahead of larger, main cracks. This behavior is attributed to the increased stresses around the main crack tip. For example, in Fig. 5 cracks can be seen adjacent to the growing, dominant crack in the colony to the right of the nucleation colony, despite the fact that the lamellar interfaces are only $\sim 23°$ from the maximum tensile stress direction.

4.1.3. Growth of the main crack from the colony of origin. Upon an increase in the applied stress range, an arrested main crack may be able to propagate out of the lamellar colony of origin and into the neighboring colonies, thus becoming a dominant, growing crack, as shown in Fig. 5. Cracks were observed to propagate out of the colony of origin by linking up with secondary cracks or cleaving through lamellae in the neighboring colonies. In all cases, the cracks which propagated were those oriented nearly perpendicular to the maximum
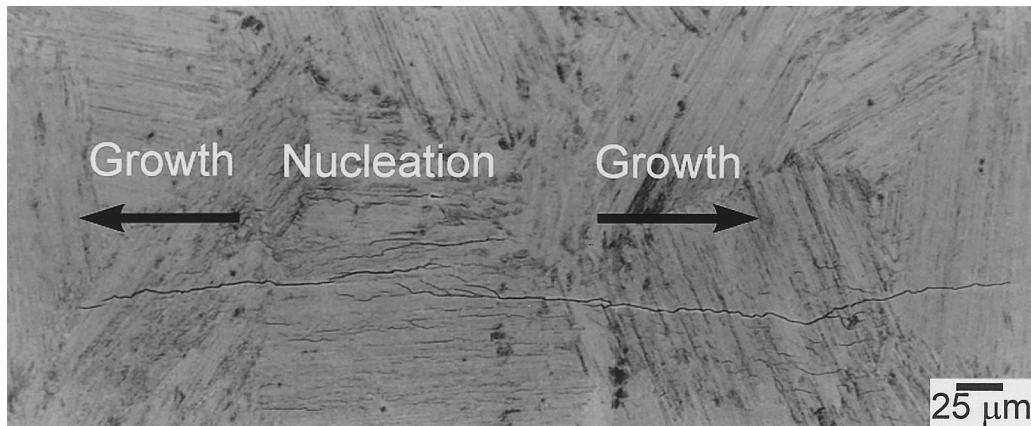

Fig. 5. A backscattered SEM micrograph showing a crack growing out of the lamellar colony of origin into the neighboring colonies. The maximum tensile stress direction was vertical with respect to the orientation of the micrograph.

tensile stress direction, while cracks along shear bands (i.e. $\beta \sim 45°$) remained arrested. This is attributed to the larger driving force associated with a crack perpendicular to the maximum tensile stress direction relative to a crack of equal size oriented at 45° to this direction.

4.2. Duplex microstructure

Similar experiments on the duplex material indicated that this microstructure is markedly more resistant to fatigue-crack initiation. Specifically:

- application of stress ranges that were sufficient to cause crack initiation readily in the lamellar microstructure (within 500–10 000 cycles) did not produce any cracks in the duplex microstructure after over 500 000 cycles;
- crack nucleation was not observed after over 500 000 cycles in the duplex material until maximum bending stresses were increased to be on the order of the ultimate tensile strength, UTS, at which time a large number of microcracks rapidly nucleated throughout the microstructure (Fig. 6) and coalesced to cause failure within ~1000–2000 cycles.

Cracks were found to nucleate at no preferred locations under these (near UTS) conditions, with cracks forming in both the γ and α_2 phases, as well as at grain boundaries. The very rapid nature of the failure process prevented any accurate determination of the growth rates for individual cracks; subsequent studies of small-crack propagation rates

in this microstructure were performed following crack initiation from EDM pits with cyclic crack growth occurring at substantially lower stress levels. Moreover, characterizing the growth rates in terms of the stress intensity for the conditions necessary to create naturally initiated cracks is questionable due to the onset of general yielding of the bend bar. It is important to note, however, that although fatigue-crack nucleation and propagation to failure occurred very rapidly, the stress levels necessary to initiate this failure process (in bending) are well above those which would ever be considered as design stress levels in structural components, as they are on the order of stresses necessary for monotonic failure. By comparison, the fatigue-failure process is initiated in the lamellar microstructure at significantly lower stress levels.

5. FATIGUE-CRACK PROPAGATION

5.1. Large cracks

It has been well documented in the literature that lamellar microstructures in γ-TiAl based intermetallics possess superior fatigue-crack growth resistance to that of duplex microstructures in the presence of large cracks (>5 mm) [4, 9, 11]. Previous results for large, through-thickness cracks in the same duplex and lamellar microstructures as studied here are shown in Fig. 7, where fatigue-crack growth rates are plotted as a function of the applied stress-intensity range, ΔK [12]. Growth rates (at a specific ΔK)
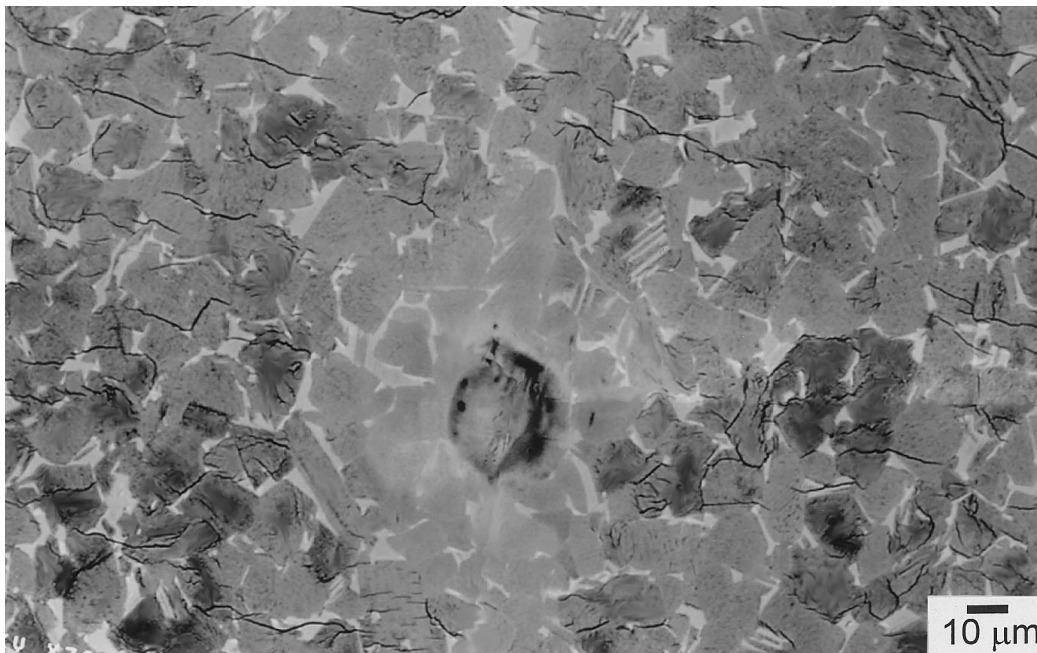

Fig. 6. A backscattered SEM micrograph showing the nucleation of many microcracks in the duplex microstructure away from the introduced laser pit. Fatigue-crack nucleation was not observed except at high stress ranges ($\sigma_{max} \sim$ UTS), where many microcracks formed (as shown) and subsequently coalesced to produce rapid failure. The maximum tensile stress direction was vertical with respect to the orientation of the micrograph.
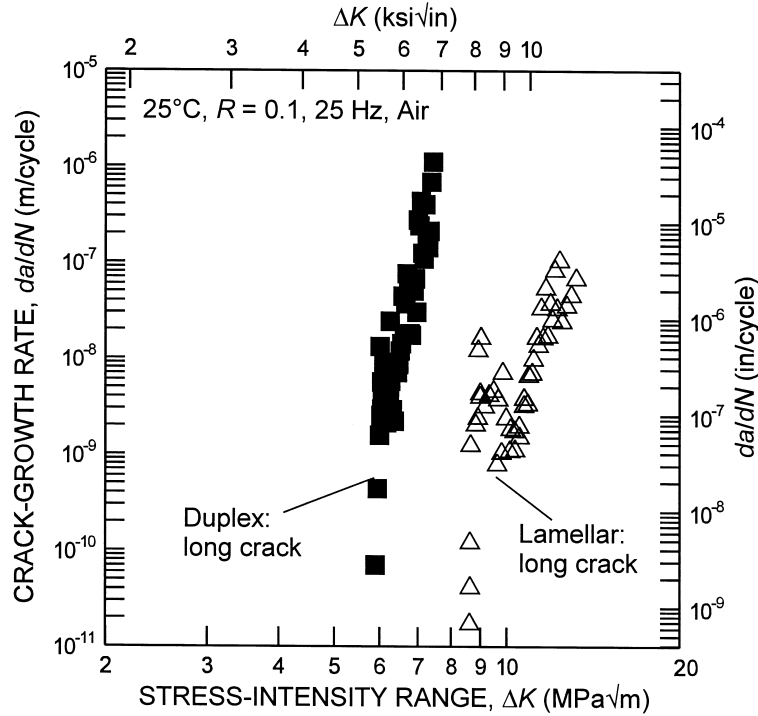
Fig. 7. Comparison of the large-crack ($c \gtrsim 5$ mm) fatigue-crack growth results, plotted as a function of the applied stress-intensity range, ΔK, for the duplex and lamellar microstructures [12, 13].

in the lamellar structure are up to five orders of magnitude lower, and threshold, ΔK_{TH}, values are some 50% higher, than in the duplex structure. This behavior has been attributed primarily to enhanced crack-tip shielding in the lamellar structure [12, 13]. Specifically, under both monotonic and cyclic loading, the formation of microcracks within the lamellae *ahead* of the crack tip leads to the formation of uncracked ("shear") ligaments; these act as very potent crack bridges leading to marked *R*-curve toughening and to superior large-crack growth resistance in fatigue (due to an effective reduction in K_{max}); additional shielding in fatigue also arises from crack closure (which leads to an effective increase in K_{min}). Whereas significant shielding by uncracked ligament bridging and closure is seen in the lamellar structure, no evidence of bridging has been reported for the duplex structure, where only minimal shielding occurs by crack closure.

The specific contribution of crack-tip shielding to the relative fatigue-crack growth resistance of the two microstructures can be readily seen by replotting the data in Fig. 7 in terms of the effective (near-tip) stress-intensity range, ΔK_{eff}, at the crack tip, i.e. after "correcting" the applied stress-intensity range for bridging and closure. As described in Ref. [12], the bridging stress intensity, K_{br}, defined as the reduction in K_{max} due to bridging, can be measured by comparing the experimentally measured compliance (of the bridged crack) to the theoretical compliance for a traction-free crack of

the same size [33]. The closure stress intensity, K_{cl}, can also be determined from specimen compliance, specifically when first contact occurs between the crack surfaces on unloading [34]. Thus, using the experimentally measured values of K_{br} and K_{cl} for these microstructures, and defining the effective stress-intensity range as

$$\Delta K_{eff} = (K_{max} - K_{br}) - K_{cl} \qquad (1)$$

the shielding contribution can be removed from the applied driving force. As shown in Fig. 8, after this is done, the remaining *intrinsic* fatigue-crack growth resistance of the two microstructures are nearly the same.

From these results, it would appear that the lamellar material only displays markedly superior fatigue-crack growth resistance when crack-tip shielding mechanisms are effective. However, it is to be expected that as crack sizes become comparable in dimension to the extent of the closure and bridging zones, the potency of these shielding mechanisms will also be reduced. This is examined below in light of the relative resistance of the duplex and lamellar microstructures to the growth of *small* fatigue cracks.

5.2. Large- vs small-crack growth

A comparison of the growth-rate behavior of small ($c \sim 25$–$300\ \mu$m) surface cracks and large ($a > 5$ mm) through-thickness cracks are shown in Fig. 9(a) and (b), respectively, for the duplex and lamellar microstructures, with the large-crack data
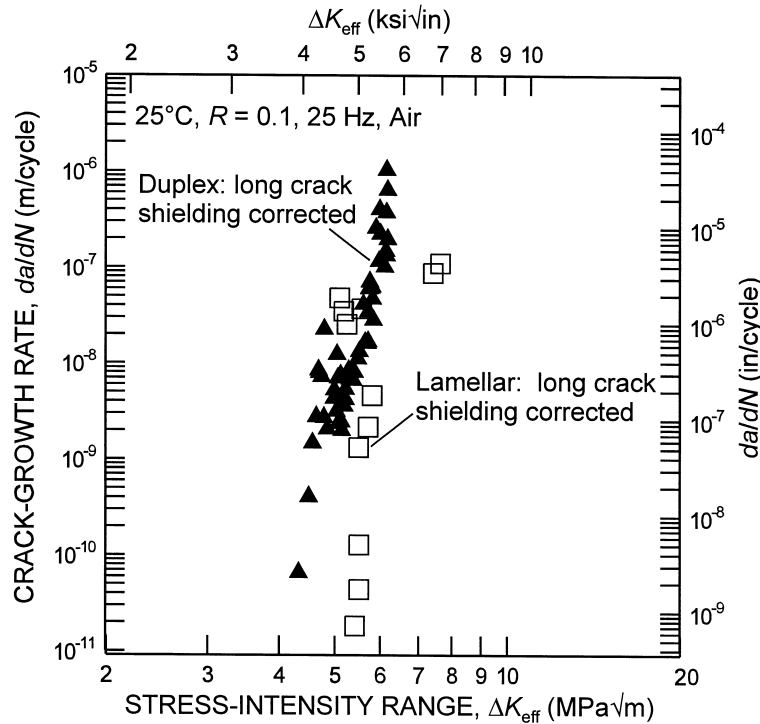
Fig. 8. Comparison of the large-crack ($c \gtrsim 5$ mm) fatigue-crack growth results for lamellar and duplex microstructures plotted in terms of the shielding "corrected" stress-intensity range, ΔK_{eff} [12, 13].

shown from both Figs 7 and 8, before and after "correcting" for shielding. Here, the small-crack data points represent the average growth rate and ΔK value over a discrete crack-growth increment; the error bars represent the range of ΔK over this increment. The small cracks from which growth rates where measured were initiated using the EDM pitting technique, and, in the case of the lamellar structure, also by natural initiation; differences in the behavior of cracks formed by these two techniques are discussed below.

In Fig. 9(a) and (b), it is apparent that at the same applied ΔK levels, the growth rates of the small cracks in both microstructures exceed those of corresponding large cracks by up to several orders of magnitude; more importantly, small-crack growth is seen at applied stress intensities below the large-crack thresholds, ΔK_{TH}. Additionally, several other points are worthy of note:

- Despite the far superior large-crack fatigue properties of the lamellar microstructure, the scatter bands of growth rates for small cracks in the duplex and lamellar materials overlap considerably (Fig. 10).
- As a consequence, the "small-crack effect", i.e. the difference between large- and small-crack results, is significantly larger in the lamellar than in the duplex microstructure.
- Despite the similarity of small-crack growth rates in the two microstructures, there is significantly more scatter in the coarser lamellar microstruc-

ture. Such scatter has been seen in previous studies of small cracks in the lamellar microstructure of this alloy [14, 21, 23]. Furthermore, small cracks in this microstructure are able to initiate and grow at significant growth rates ($\mathrm{d}a/\mathrm{d}N \sim 5 \times 10^{-8}$ m/cycle) at applied ΔK levels well below that necessary for equivalent crack-growth rates in the duplex structure.

5.3. Naturally- vs EDM-initiated cracks

The growth rates for small surface cracks in the lamellar microstructure were measured from samples in which the fatigue cracks were initiated both naturally and from EDM pits. Although microstructural damage in the vicinity of the EDM pits may be considered to affect such growth rates, the two data sets are comparable (Fig. 11), although there is less scatter with the naturally-initiated cracks.

Similar efforts were made to measure the initial growth of naturally-initiated cracks in the duplex microstructure. However, as described above, it was found that the crack-initiation resistance of the duplex microstructure was far superior to that of the lamellar microstructure. Specifically, at applied loads below the limit load, where numerous fatigue cracks would initiate in the lamellar structure, cracks simply did not initiate naturally in the duplex structure; tensile stresses on the top surface of the bend beams had to be
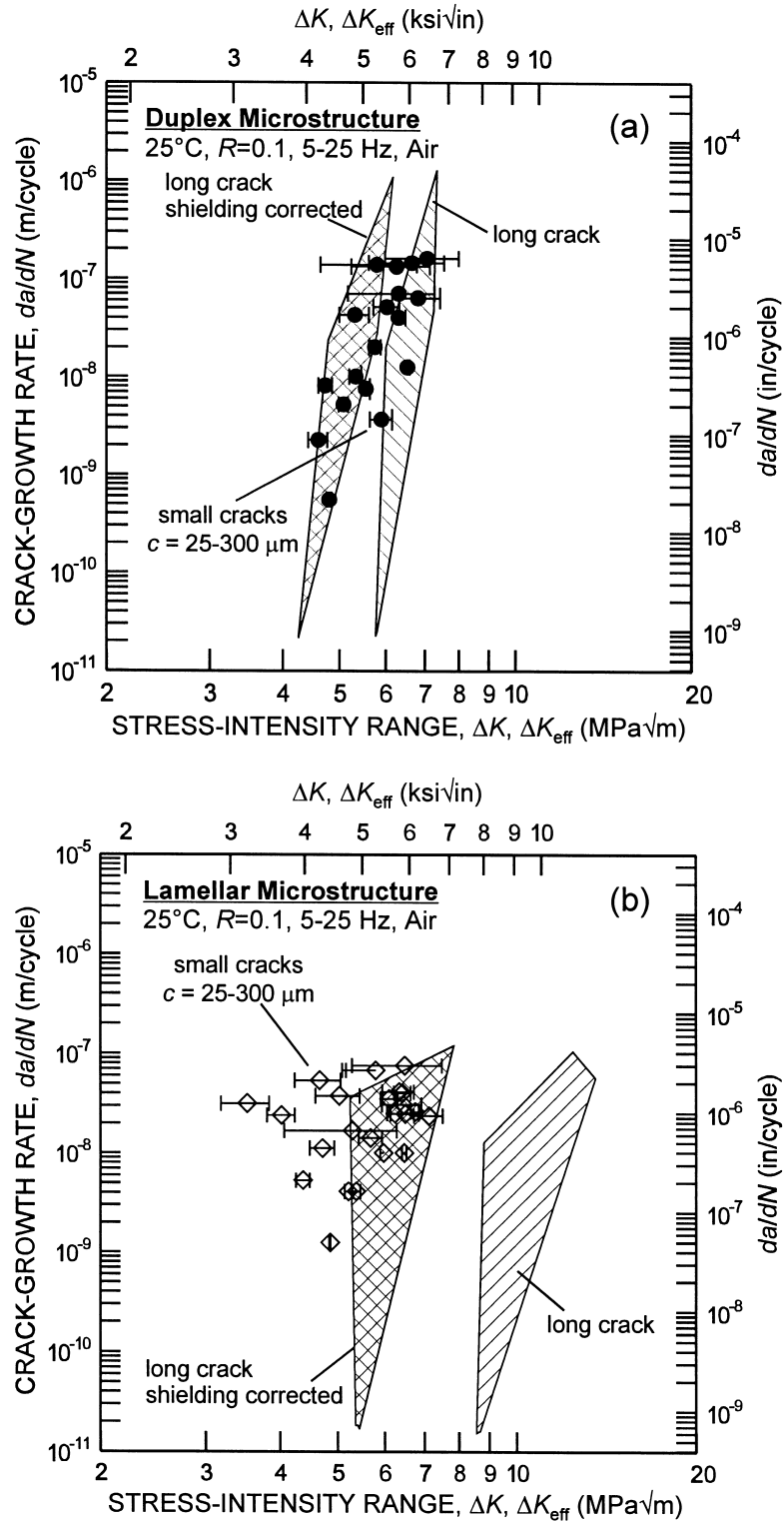
Fig. 9. Comparison of small- ($c \sim 25$–$300\,\mu$m) and large-crack growth rates for the (a) duplex and (b) lamellar microstructures, where the large-crack data (from Figs 7 and 8) are plotted in terms of both the applied ΔK and near-tip ΔK_{eff}. Error bars represent the range of ΔK values over specific growth increments.
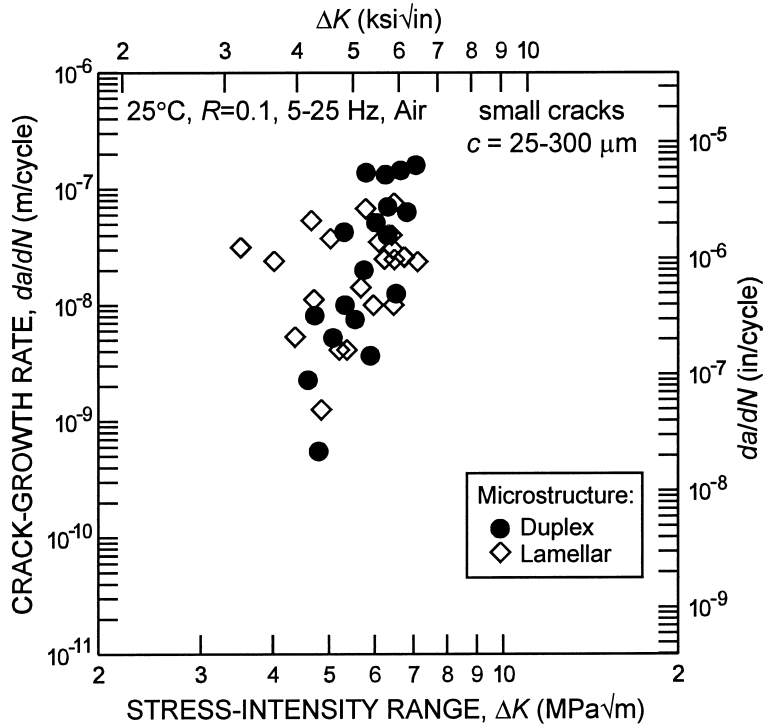
Fig. 10. Comparison of the growth rates of small cracks ($c \sim 25$–$300\,\mu$m), plotted as a function of the applied ΔK, in the duplex and lamellar microstructure.

near the UTS (coincident with gross plastic yielding of the beam) before crack initiation could be detected. For this reason, small-crack growth rates in this microstructure [Fig. 9(a)] were determined only from cracks emanating from EDM pits.
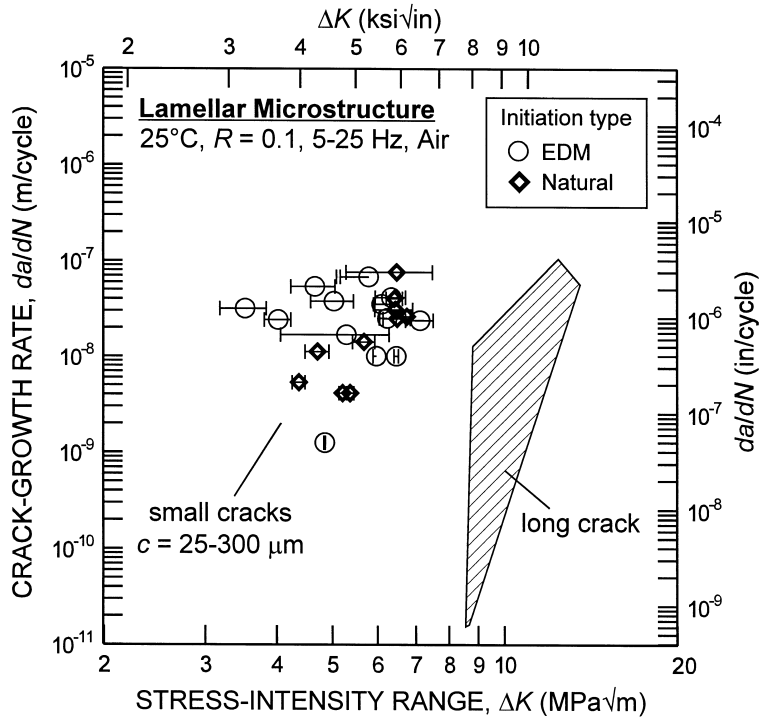

Fig. 11. Comparison of the growth-rate behavior in the lamellar microstructure of small cracks ($c \sim 25$–$300\,\mu$m) that were initiated naturally or using EDM. Error bars represent the range of ΔK values over specific growth increments.

5.4. Origin of the small-crack effect and associated design implications

5.4.1. Crack-tip shielding. Comparison of small-crack growth rates with the intrinsic large-crack growth rates (from Fig. 8), where the effect of crack-tip shielding from bridging and closure on the near-tip ΔK has been accounted for in terms of ΔK_{eff}, results in a much closer correlation between the data sets than that provided by comparison with the measured (non-shielding-corrected) large-crack data (Fig. 9). This observation suggests that the small-crack growth rates are faster than those of corresponding large cracks because of their limited wake, which does not permit the development of equilibrium bridging and closure zones behind the tip. In essence, this implies that the small-crack growth rates reflect the intrinsic crack-growth resistance, akin to the "shielding-corrected" large-crack behavior; however, this is only true where crack sizes are small compared to the shielding zone lengths (similitude limitation) yet still large compared to microstructural dimensions.

In the case of the duplex microstructure, the shielding-corrected large-crack growth rate data provide a useful reference curve for design against fatigue-crack propagation in the presence of small flaws. Examination of Fig. 9(a) indicates that the small cracks do not grow below the shielding-cor-

rected large-crack threshold, $\Delta K_{eff,TH}$. Furthermore, at a given applied ΔK, all small cracks grow at rates equal to, or slower than, large cracks at an *effective* stress intensity range, ΔK_{eff}, of equivalent magnitude. This suggests that in the duplex structure, the small-crack effect, which is observed when growth rates for large and small cracks are plotted as a function of the applied ΔK, is due solely to the lack of an equilibrium shielding zone for small cracks with limited wake size. It is thus possible to define a lower-bound threshold in the duplex microstructure, below which neither large nor small cracks (down to $c \sim 25\ \mu m$) will propagate, using crack-growth rate data acquired from standard "large-crack" samples, e.g. compact tension, plotted as a function of the closure-corrected stress intensity range, ΔK_{eff}.

The influence of crack size on the effective crack-driving force, ΔK_{eff}, is illustrated in Fig. 12, where growth rates are plotted for a single small crack in the duplex microstructure, as it propagates at a constant stress range. As the crack grows, the applied ΔK increases; however, it can be seen that the small-crack growth rates actually decrease. This inverse relationship of small-crack growth rates to applied ΔK is well known and results from the development of a crack wake and the associated shielding zone. As the shielding zone lengthens, the
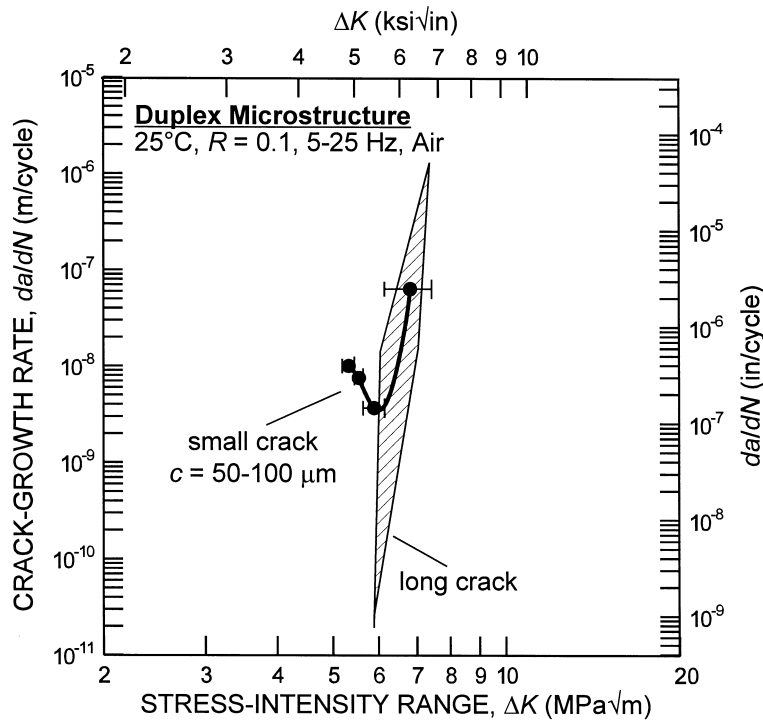

Fig. 12. Growth-rate data for a small crack ($c \sim 50-100\ \mu m$) in a specific duplex sample at a constant stress range. This crack shows an initial decrease in growth rate with increasing applied ΔK; however, once an equilibrium crack-tip shielding zone has developed, the crack exhibits the expected behavior of increasing da/dN with increasing ΔK and the data merges with that of the large fatigue cracks. Error bars represent the range of ΔK values over specific growth increments.

value of K_{cl} increases more rapidly than does the applied K_{min}; consequently the local ΔK_{eff} is decreasing even though the applied ΔK is increasing. Once the shielding zone has reached its equilibrium size, the local ΔK_{eff} values for the large and small cracks are equivalent and the data sets merge.

For the lamellar microstructure, the determination of a lower-bound threshold is not readily made using shielding-corrected large-crack data, as illustrated in Fig. 9(b). As noted above, corrections for both closure and bridging have been made to the large-crack data, as both are significant shielding mechanisms. However, in this case and in contrast to the duplex microstructure, small cracks are observed to grow at applied stress intensities below the large-crack $\Delta K_{eff,TH}$. These results suggest that the lack of an equilibrium shielding zone for small fatigue flaws, although a major factor, is not the only cause of the small-crack effect in the lamellar microstructure. The absence of a definable, lower-bound threshold below which small cracks will not propagate in lamellar γ-TiAl based intermetallics has been reported elsewhere for this particular alloy [14, 21, 23] and for others [22, 24].

For the lamellar microstructure, the measured small-crack data do not appear to merge with large-crack data over the range of crack sizes investigated

(i.e. up to a maximum surface length of $2c \sim 600~\mu m$). This implies that the improved large-crack fatigue resistance associated with the lamellar microstructure is not achieved until surface crack lengths exceed $600~\mu m$, as indicated by direct comparison of the small-crack propagation data for the two microstructures in Fig. 10. Indeed, apart from the increased scatter and lack of a definitive small-crack threshold for the lamellar structure, the growth-rate data sets for the two microstructures essentially overlap.

5.4.2. Biased microstructural sampling. In addition to being considered small in the sense of the similitude limitation, the cracks studied in the lamellar microstructure can also be regarded as small compared to microstructural dimensions (continuum limitation) since the average colony size ($\sim 145~\mu m$ diameter) is on the same order of magnitude as the cracks which were investigated ($2c \sim 50$–$600~\mu m$). This influence of the relatively coarse lamellar microstructure on small-crack behavior is apparent in Fig. 13, where the small-crack growth data are compared with shielding-corrected large-crack results. The small-crack data are further subdivided into cracks with initial surface crack lengths smaller and larger then the average colony size. From this comparison, it is apparent that all the small cracks that were observed to propagate below the shielding-corrected large-crack threshold had initial crack
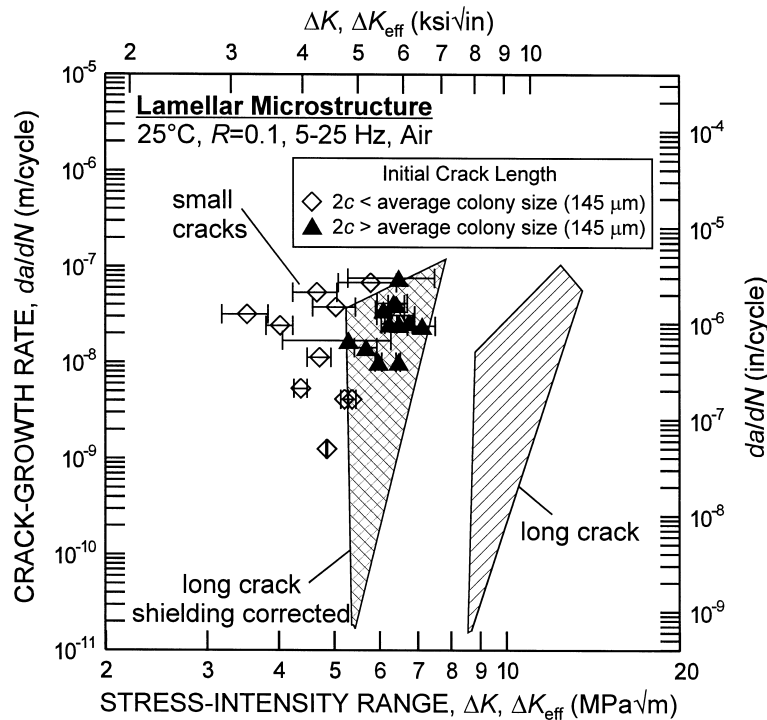

Fig. 13. Growth-rate behavior for small cracks in the lamellar microstructure compared to large-crack data as a function of ΔK and ΔK_{eff}. Note that the small-crack growth rates are only consistent with the shielding-corrected large-crack data where surface crack sizes are larger than the average colony size ($2c \gtrsim 145~\mu m$). Error bars represent the range of ΔK values over specific growth increments.

lengths *smaller* than the average colony size. Conversely, no small cracks with initial crack lengths *larger* than the average colony size grew at applied ΔK below $\Delta K_{\mathrm{eff,TH}}$. Although using the average colony size as the cutoff for this analysis is somewhat arbitrary, it does demonstrate that, for cracks contained within one or two lamellar colonies, the growth behavior is different from that observed when the crack front samples many colonies. This result is not surprising considering observations made in the present work of the strong preference for crack initiation parallel to the lamellar interface orientation (presumably a weakest-link path), and the tendency for cracks to arrest at colony boundaries. This orientation effect would then be expected to play a role in small-crack growth when only one or two lamellar colonies are sampled. For larger crack sizes, the crack is less likely to lie in an easy growth orientation relative to the microstructure in each colony the crack front samples. These observations are further supported by numerous studies that have found large cracks to grow at different rates at the same applied ΔK levels depending on the crack orientation relative to the lamellar interfaces [30–32].

In the duplex microstructure, the grain size is an order of magnitude smaller than the lamellar colony size. Consequently, effects of limited microstructural sampling would only be expected in cracks on the order of the grain size, i.e. ~ 10–$20 \,\mu m$ in length. The minimum full surface crack length investigated in this study, however, was approximately three times the average grain size.

6. FATIGUE LIFE

The crack-nucleation behavior observed for the duplex and lamellar microstructures suggests that the total fatigue life in these two materials may well be dictated by different mechanisms. Since the duplex microstructure has much higher crack-nucleation resistance, the majority of the fatigue life in duplex alloys would be expected to be spent nucleating cracks. Conversely, as crack nucleation occurs readily in lamellar alloys, the fatigue life would be expected to be dictated by the growth of small fatigue cracks. This is in agreement with results [24] on γ-based TiAl rolled sheet, where observations indicated that many cracks were nucleated very early in the fatigue life in the lamellar microstructure, whereas no cracks were observed prior to failure in the duplex structure. Similarly, fatigue life experiments ($R = 0.1$) on smooth tensile samples on both duplex and lamellar microstructures of a similar alloy (Ti–46.5Al–2Cr–3Nb–0.2W) revealed longer fatigue lives in the duplex microstructure [4].

In conclusion, although results from standard fracture-mechanics specimens containing large cracks show the lamellar microstructure to display far superior fatigue-crack propagation resistance than the duplex microstructure, this result can be deceptive. As the lamellar microstructure has much lower crack-initiation resistance and comparable small-crack growth properties, overall fatigue lives in this structure may well be shorter. For applications such as blades in gas turbines, where design must be based on the fatigue-crack threshold (i.e. no fatigue-crack growth) due to the high-frequency loading, the duplex microstructure offers more desirable properties, in the form of a definable small-crack threshold at realistic crack sizes and improved resistance to the initiation of small cracks.

7. CONCLUSIONS

Based on a study of crack-initiation and small-crack growth during the ambient-temperature fatigue of a γ-TiAl based alloy, Ti–47Al–2Nb–2Cr–0.2B (at.%), heat treated to give duplex and lamellar microstructures, the following conclusions can be made:

1. Despite the far superior large fatigue-crack growth resistance of the lamellar microstructure (due to enhanced crack-tip shielding associated with uncracked ligament bridging), crack nucleation occurred much more readily in this microstructure compared to that of the duplex microstructure. Under identical conditions (maximum stress 85% of the lamellar yield stress, $R = 0.1$), crack nucleation occurred rapidly throughout the lamellar microstructure within 500 cycles while no cracks were observed to nucleate in the duplex microstructure after 500 000 cycles.

2. Crack nucleation in the lamellar microstructure occurred preferentially at favorably oriented colonies where the lamellar interfaces were subjected to the highest tensile stresses (interfaces $\sim 90°$ to the maximum tensile stress direction) or the highest shear stresses (interfaces $\sim 45°$ to the maximum tensile stress direction). No nucleation occurred in unfavorably oriented colonies where the highest tensile stresses acted parallel to the interfaces (interfaces $\sim 0°$ to the maximum tensile stress direction). Conversely, in the duplex microstructure, crack nucleation was not observed until maximum bending stresses reached on the order of the UTS, at which time numerous microcracks rapidly formed (with no preferred microstructural orientation on location) and coalesced to cause failure within ~ 1000–2000 cycles.

3. Rates of small ($< 600 \,\mu m$) crack growth in both microstructures were found to exceed that of large cracks for a given applied (far-field) stress-intensity range. In addition, such small

cracks were observed to grow at applied stress-intensity ranges below the large-crack fatigue threshold.

4. Such "small-crack effects" could be rationalized in the duplex microstructure by comparing to large-crack results after accounting for the effect of crack-tip shielding (from crack closure). Indeed, no small cracks, in the range $c \sim 25$–$300\,\mu$m, grew at stress-intensity ranges lower than the effective large-crack threshold "corrected" for such shielding. Accordingly, the small-crack effect in the duplex structure was attributed to the lack of an equilibrium shielding zone behind the crack tip for cracks of limited wake (similitude limitation).

5. Small-crack growth rates ($c \sim 25$–$300\,\mu$m) in the coarser lamellar microstructure were comparable to the duplex microstructure, yet were subject to far more scatter. Although much of the small-crack effect in the lamellar microstructure could be explained in terms of a lack of an equilibrium shielding zone behind the crack tip, crack growth was observed below the "shielding corrected", large-crack threshold.

6. Since crack sizes in the lamellar microstructure were comparable with microstructural dimensions (i.e. the colony size), biased sampling of the microstructure led to crack growth at ΔK levels below the "shielding-corrected", large-crack threshold and to greater scatter in the lamellar small-crack data (continuum limitation).

7. Due to the difficulty of crack initiation in the duplex microstructure, it is apparent that the majority of the fatigue life for duplex alloys is spent initiating a crack of microstructural dimensions. In the lamellar microstructures, however, the relatively low resistance to fatigue-crack initiation suggests that the growth of small fatigue cracks will be an important component of the total fatigue life.

8. Although the lamellar microstructure is known to show far better *large-crack* fatigue-crack growth resistance, for applications such as gas-turbine blades where fatigue design must be based on the notion of *no* crack growth, the duplex microstructure appears to offer the more attractive properties. These include superior crack-initiation resistance and a definable lower-bound threshold for small cracks that can be obtained from "shielding-corrected", large-crack results.

REFERENCES

1. Kim, Y.-W. and Dimiduk, D. M., *J. Metals*, 1991, **43**(8), 40.
2. Kim, Y.-W., *J. Metals*, 1994, **46**(7), 30.
3. Harrison, G. F. and Winstone, M. R., in *Mechanical Behavior of Materials at High Temperature*, NATO ASI Series, ed. C. Moura Branco, R. O. Ritchie and V. Sklenicka. Kluwer Academic, Dordrecht, 1996, p. 309.
4. Larsen, J. M., Worth, B. D., Balsone, S. J. and Jones, J. W., in *Gamma Titanium Aluminides*, ed. Y.-W. Kim, R. Wagner and M. Yamaguchi. TMS, Warrendale, Pennsylvania, 1995, p. 821.
5. Liu, C. T., Maziasz, P. J., Clemens, D. R., Schneibel, J. H., Sikka, V. K., Nieh, T. G., Wright, J. and Walker, L. R., in *Gamma Titanium Aluminides*, ed. Y.-W. Kim, R. Wagner and M. Yamaguchi. TMS, Warrendale, Pennsylvania, 1995, p. 679.
6. Chan, K. S. and Kim, Y.-W., *Metall. Trans.*, 1992, **23A**, 1663.
7. Chan, K. S., *Metall. Trans.*, 1993, **24A**, 569.
8. Chan, K. S. and Kim, Y.-W., *Metall. Trans.*, 1993, **24A**, 113.
9. Venkateswara Rao, K. T., Kim, Y.-W., Muhlstein, C. L. and Ritchie, R. O., *Mater. Sci. Engng*, 1995, **A192**, 474.
10. Kumpfert, J., Kim, Y.-W. and Dimiduk, D. M., *Mater. Sci. Engng*, 1995, **A192/193**, 465.
11. Balsone, S. J., Larsen, J. M., Maxwell, D. C. and Jones, J. W., *Mater. Sci. Engng*, 1995, **A192/193**, 457.
12. Campbell, J. P., Venkateswara Rao, K. T. and Ritchie, R. O., *Mater. Sci. Engng*, 1997, **A239/240**, 722.
13. Campbell, J. P., Venkateswara Rao, K. T. and Ritchie, R. O., *Metall. Mater. Trans. A*, 1998, **30A**.
14. Campbell, J. P., McKelvey, A. L., Lillibridge, S., Venkateswara Rao, K. T. and Ritchie, R. O., in *Deformation and Fracture of Ordered Intermetallic Materials IV: Titanium Aluminides*, ed. W. O. Soboyejo, T. S. Srivatsan and H. L. Fraser. TMS, Warrendale, Pennsylvania, 1996, p. 141.
15. Badrinarayanan, K., McKelvey, A. L., Venkateswara Rao, K. T. and Ritchie, R. O., *Metall. Mater. Trans.*, 1996, **27A**, 3781.
16. Bloyer, D. R., Venkateswara Rao, K. T. and Ritchie, R. O., *Metall. Mater. Trans. A*, 1998, **30A**.
17. Nicholas, T. and Zuiker, J. R., *Int. J. Fract.*, 1996, **80**, 219.
18. Cowles, B. A., *Int. J. Fract.*, 1996, **80**, 147.
19. Ritchie, R. O. and Lankford, J., *Mater. Sci. Engng*, 1986, **A84**, 11.
20. Suresh, S. and Ritchie, R. O., *Int. Metals Rev.*, 1984, **29**, 445.
21. Campbell, J. P., Kruzic, J. J., Lillibridge, S., Venkateswara Rao, K. T. and Ritchie, R. O., *Scripta mater.*, 1997, **37**(5), 707.
22. Chan, K. S. and Davidson, D. L., in *Structural Intermetallics*, ed. R. Darolia, J. J. Lewandowski, C. T. Liu, P. L. Martin, D. B. Miracle and M. V. Nathal. TMS, Warrendale, Pennsylvania, 1993, p. 223.
23. Chan, K. S. and Shih, D. S., *Metall. Mater. Trans.*, 1997, **28A**, 79.
24. Chan, K. S. and Shih, D. S., *Metall. Mater. Trans.*, 1998, **29A**, 73.
25. Kim, Y.-W., *Mater. Sci. Engng*, 1995, **A192/193**, 519.
26. Newman, J. C. and Raju, I. S., *Engng Fract. Mech.*, 1981, **15**, 185.
27. Mahmoud, M. A., *Engng Fract. Mech.*, 1992, **41**(6), 961.

28. Mahmoud, M. A., *Engng Fract. Mech.*, 1988, **31**(2), 357.

29. Wissuchek, D. J., Lucas, G. E. and Evans, A. G., in *Gamma Titanium Aluminides*, ed. Y.-W. Kim, R. Wagner and M. Yamaguchi. TMS, Warrendale, Pennsylvania, 1995, p. 875.

30. Gnanamoorthy, R., Mutoh, Y., Hayashi, K. and Mizuhara, Y., *Scripta metall. mater.*, 1995, **33**(6), 907.

31. Davidson, D. L. and Campbell, J. B., *Metall. Trans.*, 1993, **24A**, 1555.

32. Bowen, P., Chave, R. A. and James, A. W., *Mater. Sci. Engng*, 1995, **A192/193**, 443.

33. Ritchie, R. O., Yu, W. and Bucci, R. J., *Engng Fract. Mech.*, 1989, **32**, 361.

34. Ritchie, R. O. and Yu, W., in *Small Fatigue Cracks*, ed. R. O. Ritchie and J. Lankford. TMS–AIME, Warrendale, Pennsylvania, 1986, p. 167.